Tuijin Jishu/Journal of Propulsion Technology
ISSN: 1001-4055
Vol. 45 No. 3 (2024)

Investigation of Corrosion-Induced Strains at Concrete-Rust Interface in Reinforced Concrete: A Finite Element Analysis-based Approach

Charanjeet Singh Tumrate[1,2], Shantharam Patil[3], Dhaneshwar Mishra[2,4,*]

1Department of Civil Engineering, School of Civil, Biotechnology and Chemical Engineering, Manipal University Jaipur, Jaipur 303007, India

[2]Multiscale Simulation Research Center (MSRC), Manipal University Jaipur, Jaipur 303007, India

[3]Manipal School of Architecture and Planning, Manipal Academy of Higher Education, Manipal, India

[4]Department of Mechanical Engineering, School of Automobile Mechanical and Mechatronics Engineering, Manipal University Jaipur 303007, India

Abstract: **-** The reinforced concrete thrust frames are subjected to extreme temperatures during testing of jet propulsion. The concrete-steel interface bond in reinforced concrete can be enfeebled due to the occurrence of corrosion-induced strains at the concrete-steel interface. Numerical simulations employing the finite element analysis approach can provide cost-effective and near-ideal results for comprehending the complex mechanics of corrosion-induced strains. In this work, the simulation of concrete-rust interface using the finite element analysis tool, ABAQUS 6.14 is performed. The analysis carried out by correlating the mesh size, type of mesh, and the order of solution. It was found that the quadrilateral sectional meshing, when solved with quadratic solutions provides higher accuracy. In addition, the variation in the magnitude of the principal strain due to varying rust thickness, and their location were investigated. It shows that the rust near the cover region (location of the rust) for different thicknesses gives rise to high strain values. This work can help in enhancing the design of reinforced concrete structures, thereby increasing their resilience and capacity to function effectively in corrosive environments.

Keywords*:* Concrete-rust interface, Finite element, Meshing, Principal strain, Quadratic solutions.

1. Introduction

The concrete performance under acute conditions including high temperature, radiation, etc., has been well established material for terrestrial applications [1]. The tailored concrete material to produce extraterrestrial concrete to be used for construction of launch pads and repair damaged structural components act as a resilient structural solution [2]. The occurrence of steel corrosion in reinforced concrete results in crack initiation and later crack propagation. The alkaline environment in concrete provides passivity to the steel reinforcement against corrosion. The integrity of the passive film around steel gets compromised due to the reduction of the pH in case of excess chloride ions presence or carbonation process of concrete [3]. Along with the crack width, the steel corrosion in concrete is also influenced by the crack depth and its frequency [4]. The corrosion-induced cracks can exacerbate the effects of surface cracks, leading to accelerated deterioration and potential structural problems. Crack growth and proliferate allows additional corrosive chemicals (such as water, oxygen, and chlorides) to reach the rebar and speed up the corrosion process. Furthermore, the physical bond between the concrete and the rebar is damaged by cracking and the presence of corrosion products at the contact [5] . Therefore, it is vital to monitor the structural surface cracks, and understand the mechanism of corrosion induced cracks in the reinforced concrete structures. The Artificial Intelligence (AI) based Computer Vision (CV) techniques includes image processing techniques using libraries such as OpenCV, Pytorch, Tensorflow, used to develop customized structural surface

anomaly monitoring models[6], [7], [8], [9], [10], [11], [12]. After detection of concrete surface defects, it is important to understand the source of cracks, spalling, and delamination. The corrosion failure risk of steel in concrete can be determined using numerical model by measure the breadth of the concrete fractures and calculate the length along the rebar with uniform corrosion, designated as the length of anodic zone [13]. Pitting corrosion cause serious damage to metals through targeted assaults, which is why it is still a major problem in many different sectors. Pitting corrosion is often acknowledged to be primarily caused by chloride ions (Cl-). Due to their aggressive character, they can cause localized anodic dissolution by upsetting the protective passive coating on metals [14]. Pit development and metal dissolution are accelerated by an autocatalytic process that is triggered by the hydrolysis of metal cations, turning the pit environment acidic [15]. Utilizing thick-walled cylinder models, the determination of service life of reinforced concrete structures includes the comparison of the expected cracking times with test data and evaluating the impact of various factors that affect concrete cracking times [16]. Interface components were used to describe the bonding mechanism and the expanding behavior of the rust between the bottom rebars and the concrete. A lower tensile strength of the concrete positioned at the bottom of the beam and varying corrosion rates to various interface parts differentiated the pitting and uniform corrosion from one another [17]. Finite element (FE) analysis-based modelling of concrete cracks due to rebar corrosion provides an insight between the rate of corrosion and crack propagation. In computational and mathematical point of view, it is difficult to mimic the evolution of the metal-electrolyte interface over time. Multiple pit growth, a pit-to-crack transition stage, and the propagation of one or more cracks are common features of Stress Corrosion Cracking (SCC) failures [18]. Using the Extended Finite Element Technique (XFEM), it is possible to study the effects of the transverse crack deflection angle and breadth on the diffusion process in the simulation of corrosion-induced fracture routes [19], and a three-dimensional diffusion-mechanical model of reinforced concrete with transverse cracks [20]. A new formulation for predicting dissolution-driven pitting and stress corrosion cracking capture details of the pit growth phenomena and impacting engineering practice [21]. A study conducted to compare experimental, and FE based simulated results consist of a beams of span 1200 mm and 100 mm x 150 mm rectangular cross-sections with two steel rebars of 8mm diameter spaced at 75mm c/c. The experimental deflection of 3.69mm noted at the ultimate load. When compared with FE based ABAQUS simulations, a defection of 3.54 mm were observed. An analytical mathematical model can forecast the weight loss of the reinforcing bar (WS) and the time for concrete cover (TCR) to crack in corroded reinforced concrete structures. When the recommended values of ft (concrete tensile strength) from Eq. (1) [22] are applied to the provided collection of experimental data where f_{cm} represents the cylindrical compressive strength of concrete after 28 days.

$$f_{t=0.302}\, f_{cm}^{0.67} \quad \text{MPa} \qquad (1)$$

The distribution of the corrosion level results in varying pit volume around the rebar causing tensile stress to rise, leading to concrete cracking. The TCR and WS are estimated reasonably and are in relatively good agreement with the available experimental investigations [23], [24].

It is estimated that the rust is equivalent to 6.5(pit volume) [25], [26], [27]. The pitting length along with the total mass loss increases greatly in presence of corrosion induced cracks but the correlation between the total mass loss in the pit and the maximum cross-sectional area loss is not well established [28]. The finite element-based simulation of corrosion induced cracks provides understanding of the crack propagation from the corroded rebar to the surrounding concrete. The crack pattern obtained by considering uniform corrosion using thermal analogy showed the maximum principle plastic strain for three temperature increase of 59K, 119K, and 300K. The model consist of 150 x 150 mm concrete section with a single rebar diameter of 16 mm having 20 mm cover [29]. This work investigates corrosion-induced strains at the concrete-rust interface using finite element method (FEM) simulations. It assesses the efficacy of various meshing strategies (quadrilateral vs. triangular) and solutions (linear vs. quadratic) by concentrating on maximal in-plane main strains. According to the findings, strain convergence is improved when quadrilateral meshing is used with quadratic solutions. The study also investigates the effects of rust thickness and rebar location on interface strain changes. These realizations can improve reinforced concrete structure durability and design for corrosive situations.

2. Finite element modelling of concrete rust interface

A reinforced concrete section of dimension 350mm x 600mm having four rebars of 25 mm diameter@ 75 mm c/c is simulated with a cover of 30mm and initial rust layer of 0.5 mm. For the implicit analysis considering damage plasticity model with 30mm cover, the maximum in-plan strain recorded for a triangular mesh and quadrilateral mesh were 3.667E-04 and 4.807E-04 respectively [30]. For the convergence requirement of the Abaqus based FE simulation results, combine set consisting of triangular mesh with linear and quadratic solutions and quadrilateral mesh with linear and quadratic solutions were applied. The convergence requirement of the FE simulation based results were achieved, as shown in Figure 1 for the mesh set combinations shown in Table 1. The maximum in-plan principle strain of 4.369E-04 satisfies the convergence requirement that has been achieved by using quadrilateral mesh and quadratic solutions. It is vital to understand the distribution of induced strain at the rust concrete interface due to corrosion in a reinforced concrete sections.

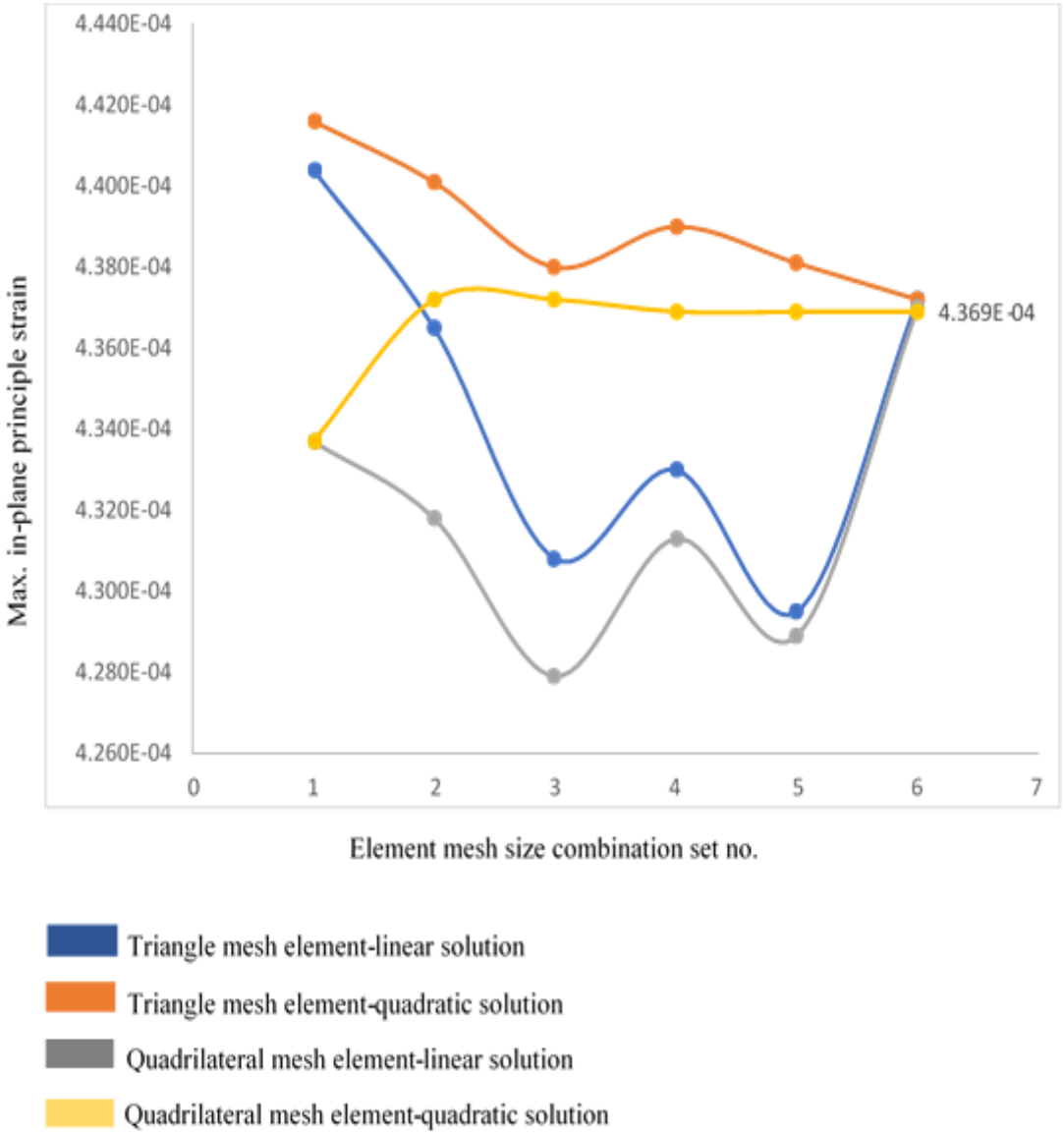

Figure 1: The Max. in-plane principle strain values (y axis) for the various triangular and quadrilateral mesh elements and FE solution types are shown with respect to the six cross section mesh size combinations set numbers (x axis).

Table 1: The concrete, rust, and rebar mesh size combinations.			
Set no.	Concrete mesh size (mm)	Rust mesh size (mm)	Rebar mesh size(mm)
1	2	1.5	1.5
2	1.5	1	1
3	1	1	1
4	1	0.5	0.5
5	0.5	0.5	0.5
6	0.5	0.05	0.05

A cross-section of M30 concrete grade with 8mm diameter steel rebar (M30S08) beam is considered. The beam is modelled using finite element based Abaqus software. The materials properties of concrete and steel is applied along with the rust properties including 120 MPa modulus of elasticity, and poison's ration of 0.4. For the Concrete Damaged Plasticity (CDP), the max. biaxial compressive stress / max. uniaxial compressive stress is 1.16 , dilation angle 31•, eccentricity 0.1 , shape factor 0.667, and viscosity parameter of 0.0001. An implicit analysis in step up process is considered with interface of steel, rust, and concrete connected using tie. For FE simulation of corrosion induced strains at concrete rebar interface for a M30S08 beam. The concrete section model with rust and steel combinations is shown in Figure 2. The study consist of three cases including four combinations of rust positioning at rebar 1, 2, 3, and 4. This provides a robust approach to determining the maximum principle strain occurrence due to corrosion induced stresses in the surrounding concrete generated at the rust-concrete interface.

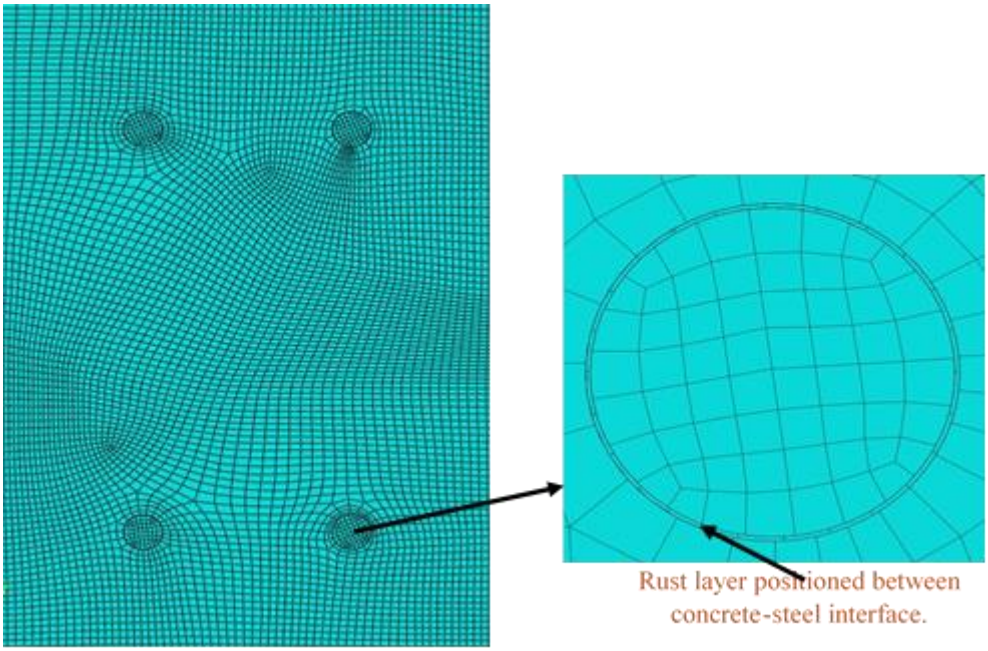

Figure 2: The M30S08 beam sectional modelling with concrete, rust and steel rebars combinations. Uniform rust around the complete rebar diameter is considered.

In another case , the concrete section model with rust and steel combinations is shown in Figure 3. Modelling rust properties at the rebar location 1, 2 ,3 ,and 4 are shown with uniform rust considered around half rebar diameter at the bottom (1 and 2) and top (3and 4) rebars.

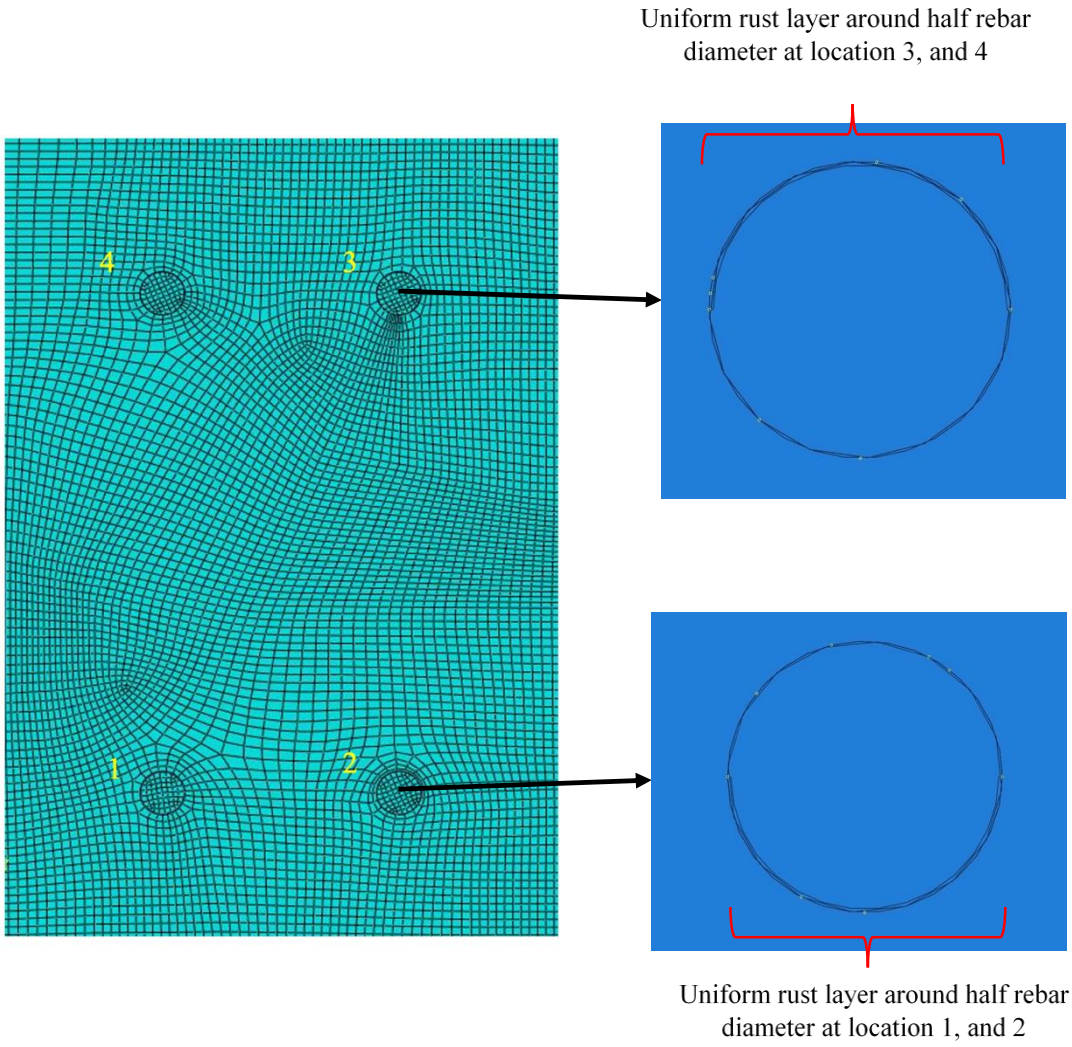

Figure 3: The M30S08 beam sectional modelling with concrete, rust and steel rebars combinations. Uniform rust considered around half rebar diameter at the bottom rebars 1,2 and top rebars 3, and 4.

3. Results and Discussion

3.1 The strain value with 0.1 mm uniform rust thickness around rebar diameter

The In-plane primary strain values are presented in Figure 4, along the vertical axis, which ranges from 5.600E-04 to 5.950E-04. On the horizontal axis, the set number representing various mesh combinations considered for concrete, rust and rebar sections are presented. Based on the rust thickness of 0.1mm, the maximum in-plane primary strain with rust modelled for only rebar 1 is represented by the blue line, for rebars 1 and 2 is represented by the orange line, for rebars 1, 2, and 3 is represented by the greyline, and for all four rebars, with rust consideration is shown by the yellow line. With distribution of the rust among all four rebars, the max. in-plane principle value is less but more critical strain hinges are formed at the concrete-rust-steel interface.

Table 2: The concrete, rust, and rebar mesh size combinations for 0.1mm uniform rust thickness.			
Set no.	Concrete mesh size (mm)	Rust mesh size (mm)	Rebar mesh size(mm)
1	2	1.5	1.5
2	1.5	1	1
3	1	1	1
4	1	0.5	0.5
5	0.5	0.5	0.5
6	0.5	0.05	0.05

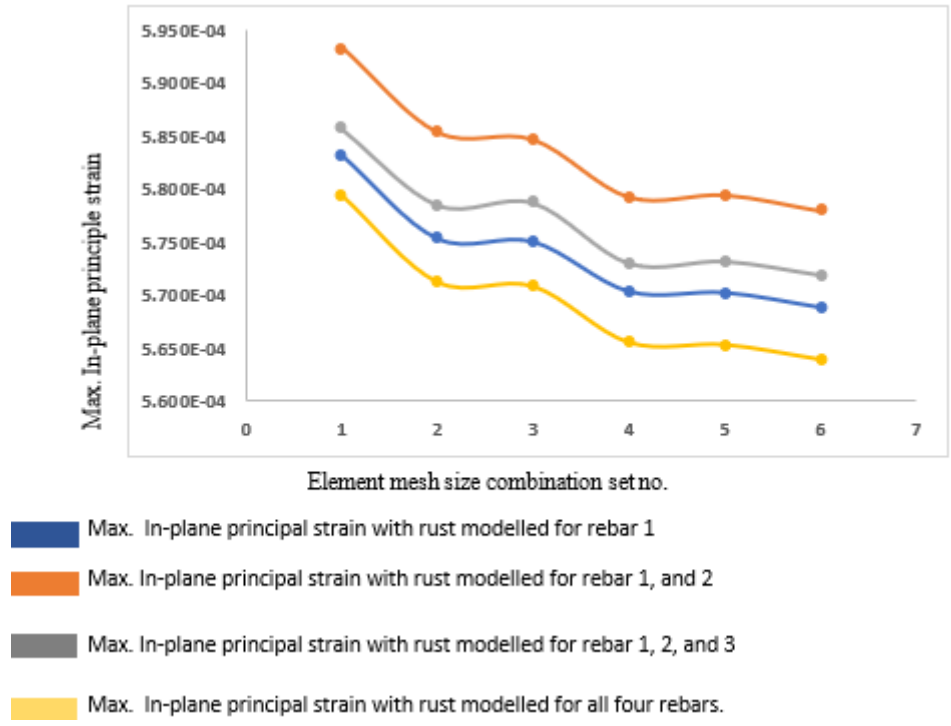

Figure 4: Six mesh combinations for concrete, rust and rebar section with max. in-plane principle strain values are plotted for the uniform rust thickness of 0.1mm.

3.2 The strain value with 0.5 mm uniform rust thickness around rebar diameter

A comprehensive representation of the Finite Element (FE) quadrilateral mesh model, shown in Figure 5, is used to simulate the M30S08 cross-section in a concrete structure with embedded rebars. The model focuses on the interactions of concrete, rust of thickness 0.5mm , and rebar elements, with a particular emphasis on the consequences of corrosion-induced strain. The left side of the figure shows a close-up of the mesh configuration, emphasizing the various mesh sizes used: 0.5 mm mesh for concrete, 0.05 mm mesh for the rust layer, and 0.05 mm mesh for the rebar. The right side of the figure shows a cross-sectional view of the model, with the max. in-plane primary strain distributed across the entire section. The strain values are color-coded, and the scale ranges from -1.882e-07 to +1.682e-04, indicating the different amounts of strain encountered by the concrete. The visual representation and intricate mesh layout provide a thorough understanding of how corrosion affects the concrete structure, highlighting important regions where strain is highest.

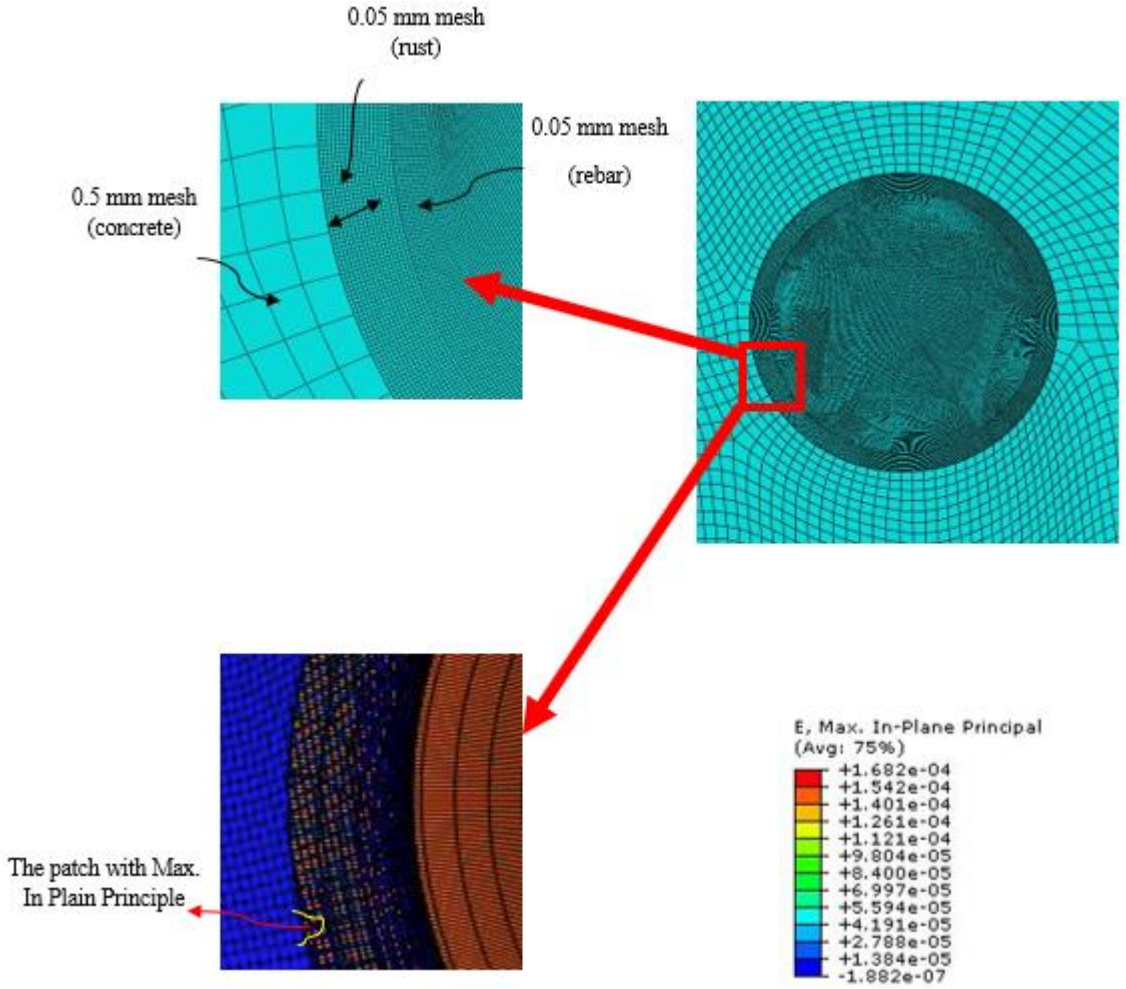

Figure 5: The concrete, and rebar FE quadrilateral mesh model replicating the M30S08 cross-section. A uniform rust layer of 0.5mm is considered to induce the external stress to the surrounding concrete in corrosion induced strain conditions.

The comparison of maximum in-plane primary strains (E) for various rust states and rebar locations are mentioned in Table 3. These strain values are plotted against rust sites at rebar positions 1, 2, 3, and 4, using three series of data points. The strain values for three rust conditions—0.1 mm uniform rust thickness around rebar diameter, 0.1 mm uniform rust thickness about half the rebar diameter, and 0.5 mm uniform rust thickness around half the rebar diameter are shown in the Table 3.

Table 3: Comparison of max. In-plane principle strains for various rust conditions applied to rebar locations.

Rust model location	0.1 mm uniform rust thickness	0.1 mm uniform rust thickness around half rebar diameter	0.5 mm uniform rust thickness around half rebar diameter
Rebar 1	4.263E-04	4.263E-04	5.689E-04
Rebar 1+2	4.101E-04	4.101E-04	5.780E-04
Rebar 1+2+3	4.394E-04	4.394E-04	5.720E-04
All rebars	4.417E-04	4.417E-04	5.640E-04

The maximum in-plane principle strains for various rust conditions applied to various rebar locations are compared in the Table 3. The three conditions, a 0.1 mm uniform rust thickness, a 0.1 mm rust thickness about half the rebar diameter, and a 0.5 mm rust thickness around half the rebar diameter are examined. Within the homogenous rust thickness of 0.1 mm around complete rebar diameter and half rebar diameter, the strain values are almost same, vary between 4.101E-04 and 4.417E-04. For the rust thickness of 0.5 mm around half rebar diameter the stain ranges from 5.64E-04 to 5.78E-04.

4. Conclusion

Formation of corrosion-induced strains at the concrete-rust interface are studied using finite element based simulation techniques. A convergence study was carried out to verify the element size, and solution type for evaluating the maximum in-plane principal strains arising from rust-induced stress at the concrete-rust interface of a reinforced concrete beam. A correlation between quadrilateral and triangular meshing with both linear and quadratic solutions has been found out. It was observed that the quadrilateral sectional meshing, when solved with quadratic solutions, achieves higher accuracy of in-plane principal strain values at the concrete-rust interface. The maximum in-plane principal strain was evaluated for several rebar configurations with a rust thickness of 0.1 mm and 0.5 mm. It assisted in understanding the relation of concrete-rust-steel interfaces under induced stresses. The variation in interface strain due to changes in rust thickness and positioning around the rebars is also analysed, providing valuable insights into the mechanics of corrosion-induced strains in reinforced concrete structures.

5. Acknowledgement

The authors would like to acknowledge the support provided by Manipal Academic of Higher Education (MAHE), Udupi, Karnataka under MAHE mobility grant. The authors would also like to acknowledge the computational facilities provided by the Multiscale Simulation Research Center (MSRC) at Manipal University Jaipur.

Reference

[1] M. Z. Naser and A. I. Chehab, “Materials and design concepts for space-resilient structures,” *Progress in Aerospace Sciences*, vol. 98, pp. 74–90, Apr. 2018, doi: 10.1016/J.PAEROSCI.2018.03.004.

[2] M. Z. Naser, “Extraterrestrial construction materials,” *Prog Mater Sci*, vol. 105, p. 100577, Aug. 2019, doi: 10.1016/J.PMATSCI.2019.100577.

[3] W. K. Green, “Steel reinforcement corrosion in concrete – an overview of some fundamentals,” *Corrosion Engineering, Science and Technology*, vol. 55, no. 4, pp. 289–302, May 2020, doi: 10.1080/1478422X.2020.1746039.

[4] F. U. A. Shaikh, “Effect of Cracking on Corrosion of Steel in Concrete,” *Int J Concr Struct Mater*, vol. 12, no. 1, pp. 1–12, Dec. 2018, doi: 10.1186/S40069-018-0234-Y/FIGURES/15.

[5] C. S. Tumrate, A. Rizal, and D. Mishra, “Modeling Crack Growth in Materials Using Finite Element Method,” *Deformation and Fracture in Materials*, pp. 194–205, Jul. 2024, doi: 10.1201/9781003359364-12.

[6] C. S. Tumrate, S. L. Vajire, and D. Mishra, “Applications of Machine Learning Techniques to Predict Behaviour of Materials,” *Deformation and Fracture in Materials*, pp. 54–66, Jul. 2024, doi: 10.1201/9781003359364-4.

[7] C. S. Tumrate and D. Mishra, “Concrete surface crack detection system through OpenCV library,” *AIP Conf Proc*, vol. 2835, no. 1, Jul. 2024, doi: 10.1063/5.0221510/3302064.

[8] C. S. Tumrate, D. K. Saini, P. Gupta, and D. Mishra, “Evolutionary Computation Modelling for Structural Health Monitoring of Critical Infrastructure,” *Archives of Computational Methods in Engineering 2022 30:3*, vol. 30, no. 3, pp. 1479–1493, Nov. 2022, doi: 10.1007/S11831-022-09845-1.

[9] C. Z. Dong and F. N. Catbas, “A review of computer vision–based structural health monitoring at local and global levels,” *Struct Health Monit*, vol. 20, no. 2, pp. 692–743, Mar. 2021, doi: 10.1177/1475921720935585/ASSET/IMAGES/10.1177_1475921720935585-IMG6.PNG.

[10] D. Feng and M. Q. Feng, “Computer vision for SHM of civil infrastructure: From dynamic response measurement to damage detection – A review,” *Eng Struct*, vol. 156, pp. 105–117, Feb. 2018, doi: 10.1016/J.ENGSTRUCT.2017.11.018.

[11] K. Malhotra, D. Mishra, and C. S. Tumrate, "Prediction of concrete compressive strength employing machine learning techniques," *Mater Today Proc*, Jun. 2023, doi: 10.1016/J.MATPR.2023.05.717.
[12] Charanjeet Singh Tumrate, Dhaneshwar Mishra, Kulwant Singh, and Dinesh Kumar Saini, "Indian Patent Office," 2023. Accessed: May 24, 2024. [Online]. Available: https://search.ipindia.gov.in/IPOJournal/Journal/ViewJournal
[13] J. H. Castorena-González *et al.*, "Modeling Steel Corrosion Failure in Reinforced Concrete by Cover Crack Width 3D FEM Analysis," *Front Mater*, vol. 7, p. 483965, Feb. 2020, doi: 10.3389/FMATS.2020.00041/BIBTEX.
[14] D. Song, W. Sun, J. Y. Jiang, H. Ma, J. C. Zhang, and Z. J. Cheng, "Corrosion Behavior of Cr Micro-alloyed Corrosion-resistant Rebar in Neutral Cl−-containing Environment," *Journal of Iron and Steel Research, International*, vol. 23, no. 6, pp. 608–617, Jun. 2016, doi: 10.1016/S1006-706X (16)30095-4.
[15] A. Feng and Y. Han, "The microstructure, mechanical and corrosion properties of calcium polyphosphate reinforced ZK60A magnesium alloy composites," *J Alloys Compd*, vol. 504, no. 2, pp. 585–593, Aug. 2010, doi: 10.1016/J.JALLCOM.2010.06.013.
[16] Y. Liang and L. Wang, "Prediction of corrosion-induced cracking of concrete cover: A critical review for thick-walled cylinder models," *Ocean Engineering*, vol. 213, p. 107688, Oct. 2020, doi: 10.1016/J.OCEANENG.2020.107688.
[17] L.-Z. Chang, J. Thorsson, and K. Lundgren, "3D modelling of the interaction between bending and corrosion-induced cracks in reinforced concrete beams," *Constr Build Mater*, vol. 411, p. 134272, Jan. 2024, doi: 10.1016/J.CONBUILDMAT.2023.134272.
[18] N. O. Larrosa, R. Akid, and R. A. Ainsworth, "Corrosion-fatigue: a review of damage tolerance models," *International Materials Reviews*, vol. 63, no. 5, pp. 283–308, Jul. 2018, doi: 10.1080/09506608.2017.1375644.
[19] A. Prashant Singh, A. Tailor, C. Singh Tumrate, and D. Mishra, "Crack growth simulation in a functionally graded material plate with uniformly distributed pores using extended finite element method," *Mater Today Proc*, vol. 60, pp. 602–607, Jan. 2022, doi: 10.1016/J.MATPR.2022.02.123.
[20] S. Yu and H. Jin, "Modeling of the corrosion-induced crack in concrete contained transverse crack subject to chloride ion penetration," *Constr Build Mater*, vol. 258, p. 119645, Oct. 2020, doi: 10.1016/J.CONBUILDMAT.2020.119645.
[21] C. Cui, R. Ma, and E. Martínez-Pañeda, "A phase field formulation for dissolution-driven stress corrosion cracking," *J Mech Phys Solids*, vol. 147, p. 104254, Feb. 2021, doi: 10.1016/J.JMPS.2020.104254.
[22] K. Bhargava, A. K. Ghosh, Y. Mori, and S. Ramanujam, "Model for cover cracking due to rebar corrosion in RC structures," *Eng Struct*, vol. 28, no. 8, pp. 1093–1109, Jul. 2006, doi: 10.1016/J.ENGSTRUCT.2005.11.014.
[23] null Rasheeduzzafar, S. S. Al-Saadoun, and A. S. Al-Gahtani, "Corrosion Cracking in Relation to Bar Diameter, Cover, and Concrete Quality," *Journal of Materials in Civil Engineering*, vol. 4, no. 4, pp. 327–342, Nov. 1992, doi: 10.1061/(ASCE)0899-1561(1992)4:4(327).
[24] by Youping Liu, I. L. Al-Qadi Richard M Barker, J. J. Brown, and J. D. Richard Walker, "Modeling the Time-to Corrosion Cracking of the Cover Concrete in Chloride Contaminated Reinforced Concrete Structures," Oct. 21, 1996, *Virginia Tech*. Accessed: Jan. 17, 2024. [Online]. Available: http://hdl.handle.net/10919/30541
[25] E. El Alami, F. E. Fekak, L. Garibaldi, and A. Elkhalfi, "A numerical study of pitting corrosion in reinforced concrete structures," *Journal of Building Engineering*, vol. 43, p. 102789, Nov. 2021, doi: 10.1016/J.JOBE.2021.102789.
[26] K. Bhargava, A. K. Ghosh, Y. Mori, and S. Ramanujam, "Model for cover cracking due to rebar corrosion in RC structures," *Eng Struct*, vol. 28, no. 8, pp. 1093–1109, Jul. 2006, doi: 10.1016/J.ENGSTRUCT.2005.11.014.
[27] Z. Zhao and L. Fu, "The probability distribution of pitting for accelerated corrosion reinforcement," *Case Studies in Construction Materials*, vol. 9, p. e00193, Dec. 2018, doi: 10.1016/J.CSCM.2018.E00193.

[28] E. G. Chen Carlos Berrocal Ingemar Löfgren Karin Lundgren, "Correlation between concrete cracks and corrosion characteristics of steel reinforcement in pre-cracked plain and fibre-reinforced concrete beams", doi: 10.1617/s11527-020-01466-z.

[29] Z. Cui and A. Alipour, "Concrete cover cracking and service life prediction of reinforced concrete structures in corrosive environments," *Constr Build Mater*, vol. 159, pp. 652–671, Jan. 2018, doi: 10.1016/J.CONBUILDMAT.2017.03.224.

[30] M. German and J. Pamin, "FEM simulations of cracking in RC beams due to corrosion progress," *Archives of Civil and Mechanical Engineering*, vol. 15, no. 4, pp. 1160–1172, Sep. 2015, doi: 10.1016/J.ACME.2014.12.010/METRICS.